Correlations among particles produced in proton interactions with emulsion nuclei at 800 GeV

L. M. Barbier, W. V. Jones, J. P. Wefel, and B. Wosiek*
Louisiana State University, Baton Rouge, Louisiana 70803

R. Holynski, W. Wolter, and K. Wozniak
Institute of Nuclear Physics, Krakow, Poland

M. M. Chernyavsky, G. I. Orlova, N. A. Salmanova, and M. I. Tretyakova
P. N. Lebedev Physical Institute of the Academy of Sciences of USSR, Moscow, Union of Soviet Socialist Republics

A. Abduzhamilov, L. P. Chernova, S. I. Gadzhieva, K. G. Gulamov, N. Litvinenko, N. S. Lukicheva, D. Mirkhodzhaeva, V. Sh. Navotny, E. A. Ravvina, N. Sh. Saidkhanov, and L. N. Svechnikova
S. V. Starodubtsev Physical Technical Institute, Tashkent, Union of Soviet Socialist Republics

N. W. Petrov
Institute of Nuclear Physics, Uzbek Academy of Science, Tashkent, Union of Soviet Socialist Republics
(Baton Rouge–Krakow–Moscow–Tashkent Collaboration)
(Received 10 July 1987)

Correlations among the produced particles in interactions of 800-GeV protons with nuclei in photographic emulsion provide evidence for nonindependent production of the secondary particles. Assuming particle production in clusters, the analysis implies an average multiplicity of about 3 charged particles per cluster.

I. INTRODUCTION

This paper reports a study of proton-nucleus interactions based upon an exposure of nuclear photographic emulsions to an 800-GeV proton beam at the Fermilab Tevatron. The analysis of the single-particle spectra has been reported previously,[1] and here we concentrate on the correlated two-particle spectra. For this analysis we include also the lower-energy data obtained in previous emulsion exposures to proton beams. The study of correlations in particle spectra can provide information on the fundamental particle production mechanisms in high-energy hadron-nucleus interactions. The dependences of correlation strengths on projectile energy, target mass, and target fragmentation provide constraints on the various models that have been developed to describe such collisions. These include the additive quark model,[2] the dual parton model,[3] the coherent tube model,[4] the hydrodynamic model,[5] the multichain model,[6] and the quark-string model.[7] Correlations among the produced particles should be seen in any model which allows for production of clusters, whether those clusters arise through uniform fragmentation of color tubes/strings or through some other mechanism. In our analysis the first three models mentioned above are used because they provide published predictions which are readily comparable to our experimental results.

In the additive quark model, the proton-nucleus interaction is treated as a superposition of multiperipheral quark-quark interactions. Hadronization of the slower quarks in this multiperipheral ladder may occur inside the nucleus leading to some cascading. In the dual parton model, a color-exchange phenomenon splits each interacting nucleon into a quark-diquark system. The projectile diquark interacts with the target nucleon valence quark, and the projectile valence quark interacts with the target nucleon diquark. In multiple collisions, other struck target nucleons interact similarly. In these superposition models, long-range correlations among the produced particles arise because of fluctuations in the number of interacting quarks (or diquarks).[3]

The coherent tube model is a collective model (like the hydrodynamic model) in which each of the quarks of the incident particle interact independently with a coherent tube of target nucleons. The size of this tube is determined by the quark-nucleon cross section. The number of interacting quarks and nucleons fluctuates in each event and must be averaged over in the calculation of the correlations.

The paper is organized as follows. Section II contains a brief description of the experiment and data analysis. In Secs. III–VI the results of the correlation analysis are presented. Section III discusses the long-range correlations, Sec. IV the two-particle short-range correlations, Sec. V the analysis of the pseudorapidity gap distributions, and Sec. VI the correlations in two angular variables. A summary and conclusions of this study are given in Sec. VII.

II. EXPERIMENTAL DATA

The data sample analyzed consisted of 1718 inelastic proton-emulsion nucleus interactions at 800 GeV. The

data were obtained by scanning the emulsions using, typically, 500 power magnification under a microscope. For each inelastic interaction the trajectories of the produced particles were measured with a precision of ± 1 μm in each of the spatial coordinates. Each trajectory was characterized by two angular variables, the emission angle θ and the azimuthal angle ϕ. As usual for emulsion experiments we use the pseudorapidity variable $\eta = -\ln(\tan\theta/2)$, where θ is the measured emission angle of the produced particle in the laboratory system. For this data set, the average number $\bar{n}_s$ of produced relativistic ($\beta \geq 0.7$) particles was $\bar{n}_s = 20.02 \pm 0.29$, and the dispersion D of the multiplicity distribution was $D = 11.98 \pm 0.25$, as discussed in Ref. 1.

The integrated two-particle correlation function[8] f_2 is related to the moments of the multiplicity distribution by $f_2 = D^2 - \bar{n}_s$. If the particles were emitted independently, i.e., if the multiplicity spectrum followed a Poisson distribution, f_2 would be zero. For our data f_2 is large and positive ($f_2 = 124 \pm 11$) which suggests that there are particle correlations in the data and indicates that the angular correlations between the produced particles should be examined.

One of the advantages of an emulsion detector is the ability to study simultaneously target fragmentation and particle production. In the usual terminology, protons knocked out of the target nucleus (which are identified by their range and ionization) are denoted by n_g and less energetic, singly or multiply charged target fragments by n_b. It has already been demonstrated that n_g is related to the average number $\bar{\nu}$ of intranuclear projectile-target nucleon collisions.[9] Thus, the data may be separated into samples with a fixed number of intranuclear collisions by fixing n_g. This permits the final state to be treated as a superposition of $\bar{\nu}$ projectile-nucleon collisions.

III. LONG-RANGE-CORRELATION STUDY

In a hadron-nucleus collision each quark-quark or quark-diquark interaction is assumed to give rise to a cluster of particles. It is the fluctuations in the number of such interactions (i.e., in the number of clusters) that gives rise to the observed long-range correlations.

To search for these we have examined the correlations between particles produced in different pseudorapidity intervals. In particular, we have examined the forward and backward multiplicities n_F and n_B, respectively. The forward and backward pseudorapidity regions were defined in the pp center-of-mass (c.m.) system, i.e., $n_F = n_s$ ($\eta_{\text{c.m.}} \geq 0$) and $n_B = n_s$ ($\eta_{\text{c.m.}} < 0$). For an 800-GeV proton incident on a proton at rest, $\eta_{\text{c.m.}} = 0$ corresponds to $\eta = 3.72$ in the laboratory system.

In Fig. 1 the observed dependence of the average number of particles produced in the forward (backward) regions is shown as a function of the actual number of particles in the backward (forward) hemisphere. Similar data[10] for pp collisions at the same c.m. energy ($\sqrt{s} \approx 39$ GeV) are included for comparison. Assuming a linear relationship, one finds that

$$\bar{n}_F = (0.31 \pm 0.03) n_B + (5.7 \pm 0.4) , \quad (1)$$

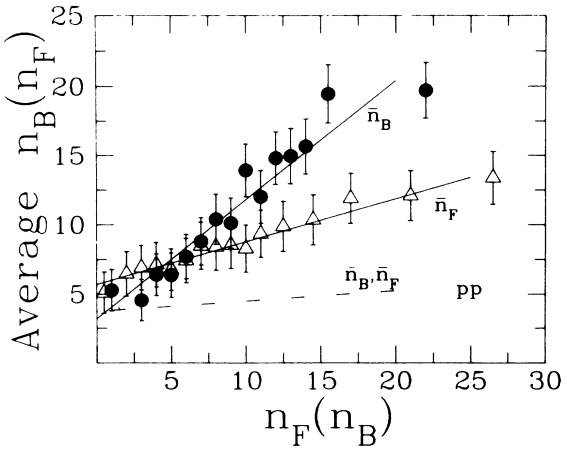

FIG. 1. Average number of particles produced in the backward (forward) region vs the number in the forward (backward) region. (●)$\bar{n}_B$ vs n_F; (△)$\bar{n}_F$ vs n_B. The dashed-dotted line represents pp data for both $\bar{n}_B$ vs n_F and $\bar{n}_F$ vs n_B.

while

$$\bar{n}_B = (0.86 \pm 0.07) n_F + (3.2 \pm 0.8) . \quad (2)$$

The slopes in these equations are referred to as the long correlation parameters. Their values indicate a strong correlation between the backward-produced particles and the forward-produced particles, but only a weak dependence exists in the opposite case. A similar effect was reported for proton-nucleus interactions at lower energies[11] but no such correlations were observed in pp collisions, where there is a symmetry between the forward and backward regions. This may indicate that the strong dependence of $\bar{n}_B$ on n_F in proton-nucleus interactions is due to multiple collisions of excited hadronic matter inside the target nucleus. In addition to this asymmetry between the forward and backward hemispheres, the correlations observed for proton-emulsion collisions are stronger than those observed in pp data. Our result for the long-range correlation strength, $b = 0.86 \pm 0.07$, is much larger than the value for pp data,[10] $b = 0.15$, at the higher CERN ISR energies of $\sqrt{s} = 62.8$ GeV.

Information about the number of particles produced in the forward and backward hemispheres for three incident energies is summarized in Table I. It is evident that the relative numbers $\bar{n}_F/\bar{n}_B$ of particles produced in the two hemispheres are constant over the energy range 67–800 GeV. Furthermore, the relative fraction of particles produced in each hemisphere scales with energy; i.e., the ratio is approximately constant when divided by $\bar{n}_s$. This indicates that $\bar{n}_F$ and $\bar{n}_B$ depend on energy in the same way as $\bar{n}_s$; i.e., they are proportional to $\ln(s)$ (Ref. 1). Note, however, that the number of particles produced in the backward hemisphere is larger than in the forward hemisphere at all energies.

To investigate the range of the forward-backward correlations, well-separated pseudorapidity windows $\Delta\eta_F$ and $\Delta\eta_B$ were used, rather than averaging over the entire hemisphere. The range of the correlations was deter-

TABLE I. Number of particles produced in forward/backward hemisphere.

Energy (GeV)	$\bar{n}_B$	$\bar{n}_F$	$\bar{n}_F/\bar{n}_B$	$\bar{n}_B/\bar{n}_S$	$\bar{n}_F/\bar{n}_S$
67[a]	5.31±0.14	4.50±0.09	0.85±0.03	0.57±0.02	0.48±0.01
200[b]	7.19±0.21	6.29±0.10	0.87±0.03	0.57±0.02	0.45±0.01
800[c]	10.79±0.35	8.85±0.29	0.82±0.04	0.54±0.03	0.44±0.02

[a]Alma-Ata–Cracow–Dubna–Leningrad–Moscow–Tashkent–Ulan Bator Collaboration, Institute of Nuclear Physics, Cracow, Report No. 787/PH, 1972 (unpublished).
[b]Alma-Ata–Leningrad–Tashkent Collaboration, E. V. Anzon *et al.*, Yad. Fiz. **22**, 787 (1975) [Sov. J. Nucl. Phys. **22**, 407 (1975)].
[c]Reference 1.

mined by dividing the available pseudorapidity intervals in each hemisphere into windows of width $\Delta\eta=1$ unit. The long-range correlation parameter was recalculated as the separation between windows increased. Figure 2 gives the slope of the dependences of $\bar{n}_B$ on n_F and $\bar{n}_F$ on n_B as the window separation increases from 0 to 4 pseudorapidity units. It is evident that the strength of the correlation is reduced by looking only in the narrow ($\Delta\eta=1$) pseudorapidity windows. Although the stronger correlations are of short range, between the adjacent windows with 0 separation, some long-range correlations exist for separations out to about 3 units of pseudorapidity.

In order to compare our results with the dual parton model, the data were analyzed with asymmetrically chosen windows separated by 1.5 units in pseudorapidity, as suggested in Ref. 3. The forward region in the pp c.m. system was assumed to be the range $0.25\leq\eta_{\text{c.m.}}\leq 1.25$ while the backward region was taken to be $-2.25\leq\eta_{\text{c.m.}}\leq -1.25$. With these choices the long-range correlation value was determined to be $b=0.41\pm0.03$. The dual parton model predicts the long-range correlation parameter to increase with energy, since it depends on the dispersion D which increases with energy. In addition, the model predictions are dependent on target mass. Some specific predictions are, for a ^{40}Ca target, $b=0.20$ at 200 GeV and $b=0.36$ at 1000 GeV; for a ^{131}Xe target, $b=0.27$ at 200 GeV and $b=0.56$ at 1000 GeV. The average atomic mass number of an emulsion target is 70, so our data at 800 GeV should lie between the ^{40}Ca and the ^{131}Xe model predictions at 1000 GeV. Therefore our value of $b=0.41\pm0.03$ is consistent with this model.

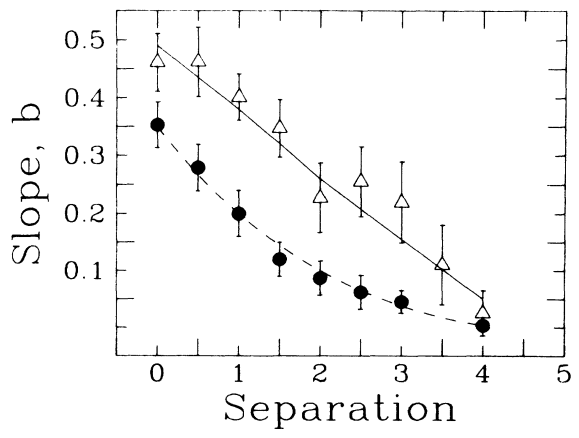

FIG. 2. Long-range correlation parameter (b) vs separation in pseudorapidity: (●)$\bar{n}_F$ vs n_B; (△)$\bar{n}_B$ vs n_F. Lines are to guide the eye.

The dual parton model assumes that the slope b is related to the number of particles emitted in a cluster by

$$b=\frac{D_{FB}^2}{D_{FF}^2}\ , \tag{3}$$

where

$$D_{FB}^2=\overline{n_F n_B}-\bar{n}_F\bar{n}_B\ , \tag{4}$$

$$D_{FF}^2=\bar{n}_c\bar{n}_F\ , \tag{5}$$

and $\bar{n}_c$ is the average number of particles per cluster. From our data a value of $\bar{n}_c=3.09\pm1.6$ is obtained.

IV. TWO-PARTICLE CORRELATION FUNCTION

The normalized two-particle correlation function is defined as

$$R_2(\eta_1,\eta_2)=\frac{\rho_2(\eta_1,\eta_2)}{\rho_1(\eta_1)\rho_1(\eta_2)}-1.0\ , \tag{6}$$

where

$$\rho_1(\eta_1)=\frac{1}{\sigma}\frac{d\sigma}{d\eta}\ , \tag{7}$$

$$\rho_2(\eta_1,\eta_2)=\frac{1}{\sigma}\frac{d^2\sigma}{d\eta_1 d\eta_2}\ , \tag{8}$$

and ρ_1 and ρ_2 are the single- and two-particle densities, respectively. Practically, R_2 can be obtained from the counted number of single particles and number of particle pairs as

$$R_2(\eta_1,\eta_2)=\frac{N_{\text{inel}}N_2(\eta_1,\eta_2)}{N_1(\eta_1)N_1(\eta_2)}-1\ , \tag{9}$$

where N_{inel} is the total number of events in the sample, N_1 (η_1) is the total number of particles at η_1, summed over all events, and N_2 (η_1,η_2) is the total number of particle pairs with one particle at η_1 and the other at η_2 in the same event, summed over all events. If there is no correlation between particles produced at η_1 and η_2 then $\rho_2(\eta_1,\eta_2)=\rho_1(\eta_1)\rho_1(\eta_2)$ and $R_2(\eta_1,\eta_2)=0$. A nonzero

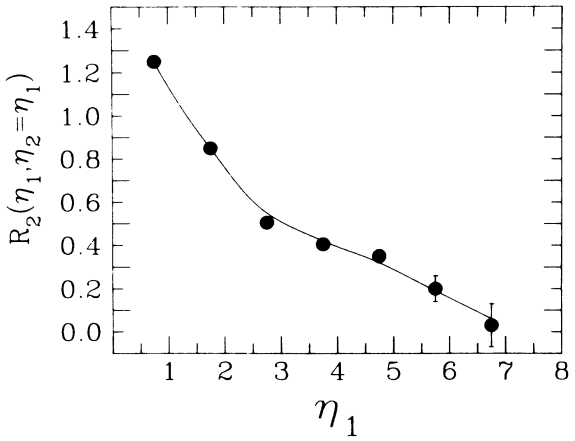

FIG. 3. Correlation function $R_2(\eta_1,\eta_2=\eta_1)$ vs η_1 for 800-GeV data. The line is to guide the eye.

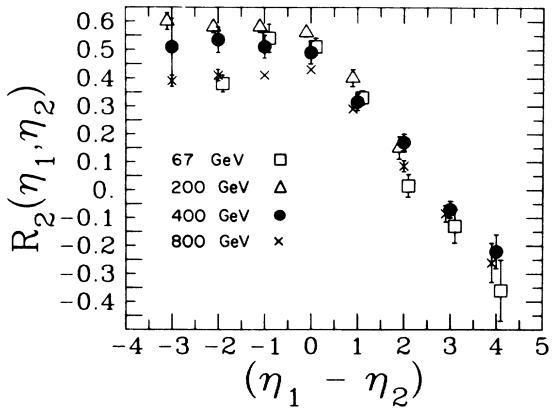

FIG. 5. Correlation function $R_2(\eta_1,\eta_2)$ for four different energies: (□) 67 GeV, (△) 200 GeV, (●) 400 GeV, (×) 800 GeV data.

value of R_2 means that particle production is a correlated phenomenon.

The plot of $R_2(\eta_1,\eta_2=\eta_1)$ as a function of η_1 in Fig. 3 shows that the probability of producing two particles close together in η is large even out to values of $\eta\approx 5$, which is near the edge of the central pionization region. Figure 4 presents $R_2(\eta_1,\eta_2)$ vs $(\eta_1-\eta_2)$ for different values of $\eta_2=2.75$, 3.75, and 4.75, which span the central region. For these three cases, the particle correlation function is positive and constant in the backward hemisphere, while in the most forward region, where energy-momentum conservation is expected to impose a negative correlation, the produced particles are indeed anticorrelated.

Figure 5 shows $R_2(\eta_1,\eta_2)$ as a function of $\eta_1-\eta_2$ for proton-nucleus collisions at 67, 200, 400, and 800 GeV. For each energy, η_2 was chosen to be the laboratory pseudorapidity of a particle emitted at 90 degrees in the equivalent *pp* c.m. frame. The features and correlation strengths are similar for all four energies. Thus, whatever mechanism is responsible for the correlations is contributing to the final multiparticle state over this entire energy range.

Figure 6 compares $R_2(\eta_1,\eta_2)$ for the 800-GeV data with the results from *pp* data[12] at nearly the equivalent center-of-mass energy. In contrast with the proton-nucleus data, the *pp* data are seen to be symmetric about zero and are consistently below the proton-nucleus data throughout the central pseudorapidity region. This indicates again the importance of multiple collisions in the target.

Figure 7 shows $R_2(\eta_1,\eta_2)$ as a function of the number of grey tracks n_g for our 800-GeV data, as well as for the additive quark model (dashed line) and for the coherent tube model (solid line). The correlation strengths for the data are seen to decrease as the number of projectile-target nucleon collisions increase. This is to be expected in the additive quark model since particles should become less correlated if there are many interactions inside

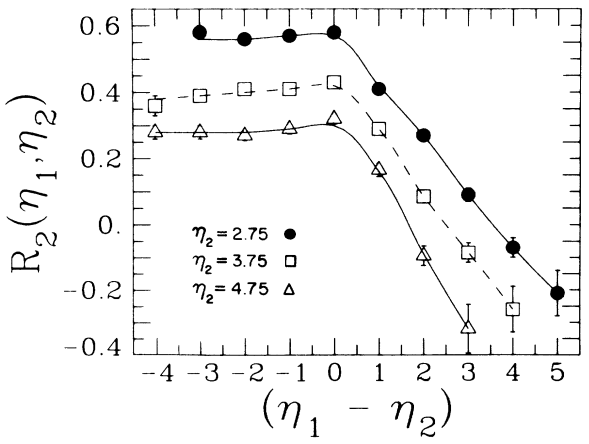

FIG. 4. Correlation function $R_2(\eta_1,\eta_2)$ vs $(\eta_1-\eta_2)$ for different η_2: (●)$\eta_2=2.75$; (□)$\eta_2=3.75$; (△)$\eta_2=4.75$.

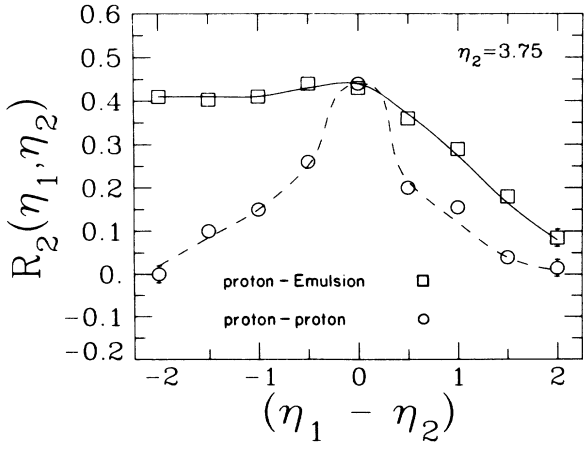

FIG. 6. $R_2(\eta_1,\eta_2)$ for proton-proton data (○) and proton-emulsion data (□), with $\eta_2=3.75$. The lines are only to guide the eye.

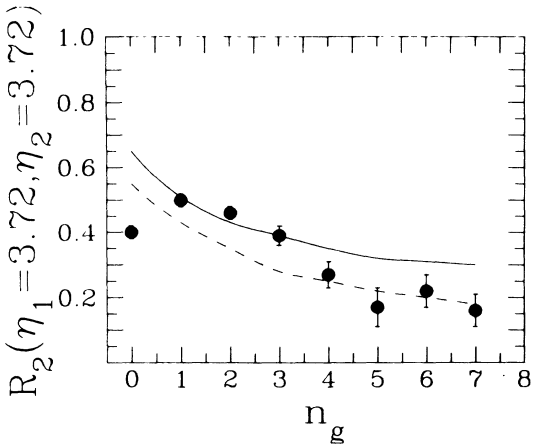

FIG. 7. Correlation function $R_2(\eta_1,\eta_2=\eta_1)$, vs n_g for $\eta_1=3.72$ in the laboratory system, compared to the additive quark model (dashed line) and the coherent tube model (solid line).

the target. In the coherent tube model R_2 decreases with n_g because the formation of hadrons from different quark tubes takes place independently, thereby "washing out" the correlation. This model is a better fit to the data for $n_g<3$, corresponding to few collisions within the target, while the additive quark model is better for $n_g>3$. Although both models explain the data reasonably well within the uncertainties, neither reproduces the small dip observed at $n_g=0$.

V. GAP DISTRIBUTIONS

Instead of studying the probabilities of producing particles at specified η values, some authors have proposed looking at the pseudorapidity "gaps" in the secondary particle distributions.[13] One may calculate a "gap distribution" for events of fixed multiplicity n by counting the number of gaps of size $r=\eta_{i+1}-\eta_i$ between adjacent particles, which are ordered in increasing values of η ($\eta_1<\eta_2<\cdots<\eta_n$). It has been shown[13] that the rapidity gap distributions for independently emitted clusters can be represented by $P(r)\approx\exp(-\rho\bar{n}_c r)$ for small r, where ρ is the density of clusters in pseudorapidity, and n_c is the average number of particles per cluster. At large r, $P(r)\approx\exp(-\rho r)$.

Adamovitch *et al.*[14] have generalized this method by skipping k particles and calculating a gap distribution for fixed values of k, i.e., $r(k)=\eta_{i+k+1}-\eta_i$. For gaps containing k particles (charged gaps) it was found[15] that the position of the peak $r_{\max}$ of the gap distributions $P(r,k)$ depends on the cluster multiplicity and cluster density as $r_{\max}=k/[\rho\bar{n}_c+(2k-1)/2k]$.

In Figs. 8 and 9 the pseudorapidity gap distributions for both charged ($k\neq0$) and uncharged ($k=0$) gaps are presented. The $k=0$ case has a different shape from the higher-order k distributions, as is seen in Fig. 8(a) where the gap distributions for $k=0$, 3, and 10 are shown for the 800-GeV data. The $k=0$ distribution shown in Fig.

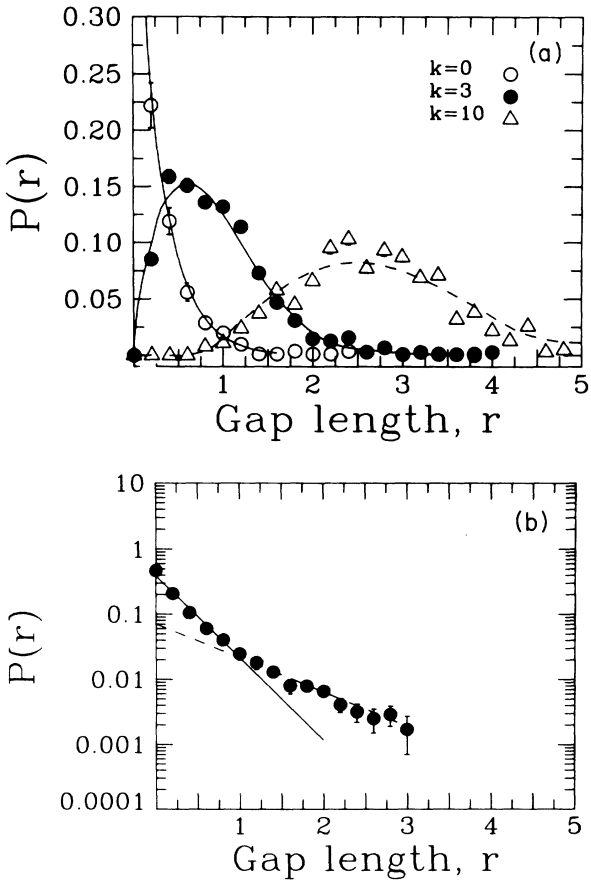

FIG. 8. (a) Gap-length distributions for $k=0$, 3, and 10 for events with $n_s=20$. The $k=0$ distribution extends to higher values as r goes to zero. The curve for $k=0$ is a fit to an exponential. The curves for the $k=3$ and 10 distributions are fits to sixth-order polynomials. (b) Gap-length distribution for $k=0$ summed over all values of n_s. The slope of the solid line for small r is 3.07 ± 0.2, while for large r the slope of the dashed line is 1.2 ± 0.1.

8(a) is best fit ($\chi^2/\mathrm{DF}=0.03$) to an exponential curve for small r:

$$P(r)=(0.46\pm0.13)e^{-(3.3\pm0.2)r}, \tag{10}$$

which implies $\rho\bar{n}_c=3.3\pm0.2$. Figure 8(b) illustrates the behavior at both large and small r for the case $k=0$, summed over all values of n_s. The slope of the exponential distribution for large r ($r>1.2$) is 1.2 ± 0.1 which is the cluster density. This value is slightly larger than the previously reported value[16] of $\rho\approx1$. When particles are widely separated, then the particle separation should be equal to the average cluster separation from which we deduce the minimum cluster separation to be the point where $P(r)$ assumes its large r behavior. In this case, the maximum cluster size is seen to be $r\approx1.2$.

From the position of the peaks of the charged gap distributions in Fig. 8(a) we find $\rho\bar{n}_c=4.07\pm0.21$ and $\rho\bar{n}_c=3.05\pm0.11$ for $k=3$ and 10, respectively. Evalua-

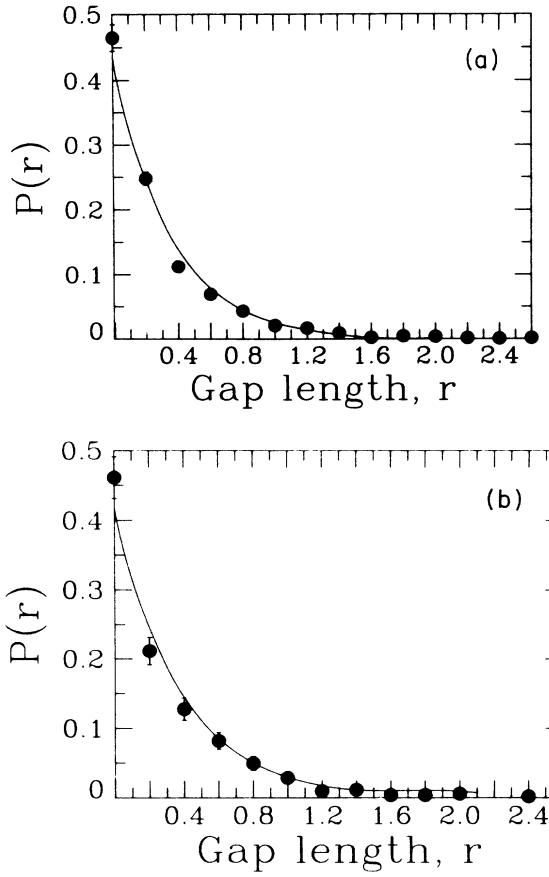

FIG. 9. (a) Gap-length distribution for 200-GeV data for $k=0$ and fixed multiplicity $n_s=14$. The curve shown is a fit to an exponential. (b) Gap-length distribution for 400-GeV data for $k=0$ and fixed multiplicity $n_s=16$. The curve shown is a fit to an exponential.

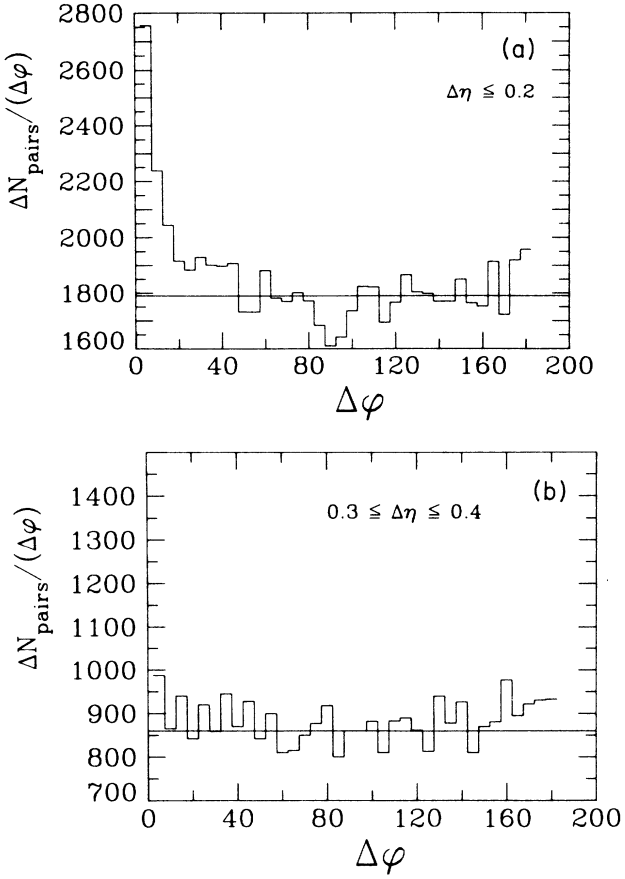

FIG. 10. (a) Number of pairs produced with $|\Delta\eta|<0.2$ vs separation in azimuthal angle ϕ, in $\Delta\phi=5°$ bins. (b) Number of pairs produced with $0.3\leq|\Delta\eta|\leq 0.4$ vs separation in azimuthal angle ϕ, in $\Delta\phi=5°$ bins.

tions of the cluster multiplicity summed over all n_s for distributions with $k=0$, 1, 2, 3, 4, 5, and 10, yield an average value of $\rho\bar{n}_c=3.35\pm0.44$. We find then that $\bar{n}_c=2.8\pm0.5$ using our experimentally determined values of 1.2 ± 0.1 for the cluster density in pseudorapidity.

The calculated $k=0$ gap distributions for 200- and 400-GeV proton-emulsion data are presented in Figs. 9(a) and 9(b). Again using an exponential fit with a value of $\rho=1.2$ from the 800-GeV data, the cluster multiplicities are, respectively, $\bar{n}_c=2.35\pm0.15$ at 200 GeV and $\bar{n}_c=2.16\pm0.16$ at 400 GeV. Consequently, it appears that the cluster size is approximately the same at all three energies.

VI. PAIR PRODUCTION

The spatial distribution of the produced particles was examined in order to search for close pairings of the secondaries. The distribution of the azimuthal separation $dN/d(\Delta\phi)$ of two particles emitted close to one another in pseudorapidity is shown in Fig. 10(a). There is a significant peak at $\Delta\phi<30°$, with 334 pairs/bin being observed above the uniform level of 1790 pairs/bin, as determined by the average number of pairs measured for $\Delta\phi>30°$. The excess of close pairs can be measured in terms of $w=N_{\rm pair}/N_t$, where $N_{\rm pair}$ is the number of pairs with $\Delta\eta\leq0.2$ and $\Delta\phi\leq30°$ above the uniform level, and N_t is the total number of pairs in the analyzed sample. For the 800-GeV data w is equal to 3%. The large peak at small $\Delta\phi$ disappears if particles are produced far apart in pseudorapidity, as illustrated in Fig. 10(b) for $0.3\leq|\Delta\eta|\leq0.4$. In comparison, there have been several reports of close pairing of secondaries in nucleus-nucleus collisions,[17] with w values up to about 10%, significantly above the present results.

VII. SUMMARY AND CONCLUSIONS

The correlations between the particles produced in 800-GeV proton-emulsion interactions have been studied and compared with lower-energy proton-emulsion data, with *pp* data, and with available model predictions.

The observed long-range correlations are significantly stronger than the correlations observed in proton-proton data, and they agree with the dual parton model predictions. Using this model and the measured value of the

long-range correlation parameter b, an average cluster size of about 3.1 particles is indicated. This value is consistent with results from the analysis of the pseudorapidity gap distributions, which yield a cluster size of about 2.8 particles, the average from the analysis of the distributions for gaps with $k=0$, 1, 2, 3, 4, 5, and 10. The $k=0$ gap distribution in Fig. 8(b) shows the cluster range to be <1.2 units of η. Since the long-range correlations shown in Fig. 2 extend to at least 3 pseudorapidity units, it appears that correlations may exist between clusters.

The two-particle correlation function R_2 is positive except in the extreme projectile-fragmentation region. Furthermore, in the backward hemisphere, R_2 is much larger than in pp interactions. This probably reflects multiple scattering of the projectile in the target. The fact that R_2 is essentially the same for 200- and 400-GeV proton-emulsion collisions, where $\bar{\nu}$ is the same, supports this conclusion. A comparison of R_2 vs n_g with the additive quark model and coherent tube model shows that both models are roughly consistent with the data.

The experimental multiplicity distribution indicates positive correlations among the produced particles. It can be described by a negative-binomial distribution[1] (NBD) which Giovannini and Van Hove[18] have shown is consistent with the idea of cluster production. In this picture, when $\bar{n} \gg K$, a parameter of the NBD ($K=3.22$ for our data), the number of particles per cluster is

$$\bar{n}_c \approx \bar{n}/[K \ln(\bar{n}/K)] + 1/[\ln(K/\bar{n})] , \quad (11)$$

which results in $\bar{n}_c = 2.85 \pm 0.07$.

To conclude, we have presented strong evidence for the production of particles in clusters in proton-nucleus collisions. If independent cluster emission is assumed, the 800-GeV data consistently imply a size of ≈ 3 charged particles per cluster and on average 6–7 clusters are produced per interaction.

ACKNOWLEDGMENT

This work was supported in part by the NSF under Grants Nos. PHY-864315 and PHY-8304003.

*On leave of absence from the Institute of Nuclear Physics, Krakow, Poland.

[1] Y. A. Abdurazakova *et al.*, Acta Phys. Pol. B **18**, 249 (1987); A. Abduzhamilov *et al.*, Phys. Rev. D **35**, 3537 (1987).

[2] G. V. Davidenko and N. N. Nikolaev, Yad. Fiz. **24**, 772 (1976) [Sov. J. Nucl. Phys. **24**, 402 (1976)].

[3] A. Capella and J. Tran Thanh Van, Phys. Lett. **93B**, 146 (1980).

[4] V. R. Zoller, Yad. Fiz. **37**, 721 (1983) [Sov. J. Nucl. Phys. **37**, 430 (1983)].

[5] E. M. Friedlander and R. M. Weiner, Phys. Rev. D **28**, 2903 (1983); K. Wehrberger, D. Syam, and S. Raha, *ibid.* **34**, 294 (1986).

[6] K. Kinoshita, A. Minaka, and H. Sumiyoshi, Prog. Theor. Phys. **61**, 165 (1979).

[7] B. Andersson, G. Gustafson, G. Ingelman, and T. Sjostrand, Phys. Rep. **97**, 31 (1983).

[8] J. D. Jackson, in *Phenomenology of Particles at High Energies,* edited by R. L. Crawford and R. Jennings (Academic, London, 1974), p. 96.

[9] J. Babecki and G. Nowak, Institute for Nuclear Physics, Krakow, Report No. 1050, 1979 (unpublished).

[10] S. Uhlig *et al.*, Nucl. Phys. **B132**, 15 (1978).

[11] B. Wosiek, Acta Phys. Pol. B **8**, 493 (1977).

[12] V. Cavassinni, *et al.*, Z. Phys. C **21**, 299 (1984).

[13] C. Quigg, P. Pirila, and G. H. Thomas, Phys. Rev. Lett. **34**, 290 (1975).

[14] M. N. Adamovitch *et al.*, Nuovo Cimento **33A**, 182 (1976).

[15] A. M. Gershkovich and I. M. Dremin, Sov. Phys. Lebedev Institute Rep. **1**, 5 (1976).

[16] S. Pokorski and L. Van Hove, Acta Phys. Pol. B **5**, 229 (1979); D. Snider Phys. Rev. D **11**, 140 (1975).

[17] Y. Takahashi and S. Dake, Nucl. Phys. **A461**, 263 (1987); P. S. Freier and C. J. Waddington, in *Cosmic Rays and Particle Fields—1978,* proceedings of the Bartol Conference, edited by T. K. Gaisser (AIP Conf. Proc. No. 49) (AIP, New York, 1979); W. V. Jones, S. D. Hunter, and Evi Brink IV, in *Proceedings of the Seventeenth International Cosmic Ray Conference,* Paris, France, 1981 (CEN, Saclay, Paris, 1981), Vol. 5, p. 67.

[18] A. Giovannini and L. Van Hove, Z. Phys. C **30**, 391 (1976).